(Received 24 December 2025, Accepted 22 January 2026, Scheduled 11 February 2026)

Wideband GCPW-Fed Coplanar Vivaldi Antenna with Low Cross-Polarization

Yiqing Gao[1], Zhao Bai[1], Hongcheng Zhou[1,2,*], Changhai Hu[3], Zhongming Yan[1,2], and Yu Wang[1,2]

[1]*School of Electrical Engineering, Southwest Jiaotong University, Chengdu 611756, China*
[2]*Key Laboratory of Magnetic Suspension Technology and Maglev Vehicle, Ministry of Education School of Electrical Engineering, Southwest Jiaotong University, Chengdu 610031, China*
[3]*School of Information Science and Technology, Southwest Jiaotong University, Chengdu 611756, China*

ABSTRACT: The traditional microstrip-fed Vivaldi antenna has the disadvantage of a high cross-polarization level owing to the nonparallelism between the electric field and the antenna plane. Based on the balanced E-field distribution property of the grounded coplanar waveguide (GCPW) structure, this paper proposes a planar ultra-wideband Vivaldi antenna with low cross-polarization. The measured results confirm that an enhanced impedance bandwidth of 159.54% is achieved in the range of 2.01–17.86 GHz ($|S_{11}| < -10$ dB) with a 4–6 dB improvement in cross-polarization over a traditional Vivaldi antenna. In addition, the proposed antenna has a maximum gain of 9.9 dBi within the size of 88.2 mm $\times$ 107.3 mm $\times$ 1 mm. Owing to the advantages of ultra-wideband, low cross-polarization ratio, stable radiation patterns, and high gain, the proposed method can be widely applied in UWB communication and multifunctional integrated RF systems.

1. INTRODUCTION

With the rapid development of modern wideband systems, owing to their wide operational bandwidth [1, 2], linear polarization, compact planar configuration [3], light weight [4], low fabrication cost [5], and good radiation characteristics, Vivaldi antenna has been extensively studied and widely applied in radar imaging, microwave measurement, wireless monitoring, and communication systems [6]. After decades of development, Vivaldi antennas can be divided into coplanar, antipodal, and balanced antipodal Vivaldi antennas. A typical coplanar Vivaldi antenna is a traveling wave antenna proposed by Gibson in 1979 [7], which can be directly fed by a coaxial line or microstrip line. The direct-feed structure is simple and efficient, but limits the operating bandwidth. An antipodal Vivaldi antenna (AVA) was proposed by Gazit to improve the operating bandwidth [8]. However, one drawback of the AVA is that the cross-polarization level is proportional to the profile. Because the conductor planes are located on different sides of the substrate, the electric field is not parallel to the antenna plane, which results in a high level of cross-polarization. To achieve low cross-polarization, Langley et al. proposed a balanced AVA (BAVA) [9]. Owing to the symmetry of the structure, the vector sum of the E-fields from the middle-layer metal to the top-layer metal and the bottom-layer metal is parallel to the antenna plane, which significantly reduces the cross-polarization level [10–12]. However, the BAVA has a three-copper-layer structure, which is demanding and costly to fabrication. Besides, patches [13] and slots [14] can be loaded on the edges of a Vivaldi antenna to improve the low-frequency radiation characteristics, which cannot reduce the cross-polarization level because the skew of the E-field in the flared slot does not decrease.

In recent years, many novel improvements based on coplanar Vivaldi antennas have been presented for low cross-polarization. Some studies have focused on controlling the current on the antenna, such as low-profile "bunny-ear" antenna [15] and sliced notch antenna [16–18]. A "bunny-ear" antenna is much shorter than traditional Vivaldi ones with negligible longitudinal current, hence bringing about lower cross-polarization [16, 17]. The sliced notch antennas are based on the principle proposed by Lee et al. that the cross-polarization behavior is essentially controlled by the ratio of the vertical-to-horizontal current and not strictly by the antenna profile [15]. However, the design process is complex and time-consuming. Other studies achieved low cross-polarization by optimizing the antenna excitation method. Qi and Liu proposed a differential-fed Vivaldi antenna [19], in which the cross-polarized E-field component is reduced owing to the symmetric configuration with a differential feeding arrangement; however, the improved frequency band is very narrow.

In this study, a low cross-polarization Vivaldi antenna fed by a grounded coplanar waveguide (GCPW) is proposed. Unlike prior GCPW-fed designs that often focus solely on impedance matching or require multi-layer stacks for polarization purity, the proposed structure achieves a favorable balance among wideband performance, cross-polarization suppression, and fabrication simplicity within a single substrate layer. The geometry of the proposed antenna is described in Section 2. The simulated and experimental results are presented in Section 3. In conclusion, the proposed antenna has a low

* Corresponding author: Hongcheng Zhou (zhouhc@swjtu.edu.cn).

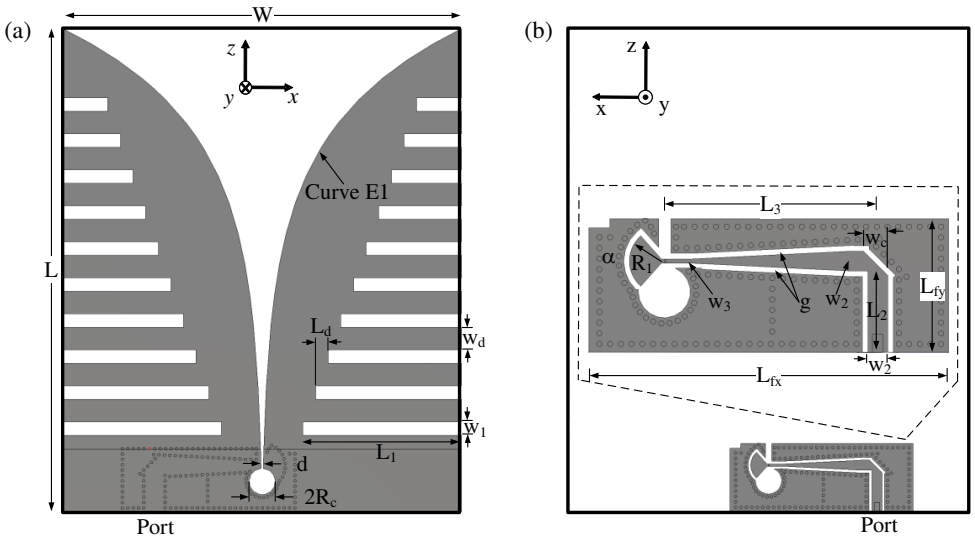

FIGURE 1. Geometry of the proposed Vivaldi antenna. (a) Front view. (b) Back view.

cross-polarization level, high gain, and stable radiation patterns over a wide operating frequency band, making it a potential candidate for ultra-wideband (UWB) communication and multifunctional integrated radio frequency (RF) systems.

2. ANTENNA DESIGN

The geometry of the proposed low cross-polarization Vivaldi antenna is shown in Fig. 1, where the *xz*-plane and *yz*-plane are referred to as the E- and H-planes, respectively. The antenna consists of two exponential radiation patches with ten slots loaded on the edge and a GCPW-to-slotline transition as the feeding structure, which is fabricated on a double-sided copper-clad Rogers RO4003C substrate (permittivity $\varepsilon_r = 3.55$, loss tangent $\tan\delta = 0.0027$) with a thickness $t = 1$ mm. The dimensions of the proposed antenna are 88.2 mm × 107.3 mm × 1 mm, and the relative dimensions are $0.72\lambda_0 * 0.59\lambda_0 * 0.007\lambda_0$, where λ_0 is the free space wavelength at the lowest operating frequency. The key optimized parameters of the antenna are specified as follows: $d = 0.5$ mm, $R = 2.9$ mm, $W_1 = 3$ mm, $L_1 = 35.2$ mm, $W_d = 5$ mm, $L_d = 2.8$ mm, $W_2 = 2.2$ mm, $W_3 = 0.5$ mm, $R_1 = 3.8$ mm, $g = 0.6$ mm.

As shown in Fig. 1(a), the exponential patches are connected to a circular cavity by a short slotline with a width $d = 0.5$ mm. The circular cavity with a radius $R_c = 2.92$ mm acts as an open-circuit to provide a good impedance match. The exponential curve E1 employed in this design can be described by:

$$z(x) = C_1 e^{(Rx)} + C_2 \tag{1}$$

where $C_1 = 0.5261$, $C_2 = -0.2745$, $R = 0.04557$. Ten slots with linearly decreasing lengths are inserted symmetrically on the left and right edges of the antenna, which are used to improve the low-frequency radiation characteristics.

As illustrated in Fig. 1, the antenna is fed by a GCPW-to-slotline transition structure, which is formed by a 50 Ω GCPW with a 90° bend, a linear tapered GCPW, and a radial stub on the back of the antenna, together with the short slotline and circular cavity on the front. An SMA connector was welded to the 50 Ω GCPW with width $w_2 = 2.2$ mm. The 90° bend is a chamfered bend with a width $w_c = 2.7$ mm, because the chamfered bend with $w_c/w_2 = 1.1$–1.25 can minimize the reflection from 90° bend. The linear tapered GCPW was used for impedance transformation from 50 to 130 Ω. At the terminal of the GCPW, an open-end was employed for broadband impedance matching.

To characterize the polarization behavior of an antenna, a common metric is cross-polarization ratio (CPR) [20]:

$$CPR(\theta,\varphi) = \frac{|E_{cross}(\theta,\varphi)|^2}{|E_{co}(\theta,\varphi)|^2} \tag{2}$$

where $|E_{cross}|^2(|E_{co}|^2)$ represents the cross-(co-)polarized field power density components of the radiated far fields. Following Ludwig's third definition, the co-polarized component E_{co} is defined as the E-field parallel to the intended polarization direction (x-axis), and the cross-polarized component E_{cross} is the orthogonal component (y-axis). In this work, the CPR is evaluated in the two principal radiation planes: the E-plane (x-z plane, $\varphi = 0°$) and the H-plane (y-z plane, $\varphi = 90°$). For the quantitative comparison of co- and cross-polarized fields presented in Section 3, the maximum relative difference within the main beam (angular range of $|\theta| \leqslant 60°$) is reported at discrete frequencies of 2, 6, 12, and 18 GHz, which represent the low, mid-low, mid-high, and high bands, respectively. The overall CPR trend across the entire operating band is analyzed using the value at boresight ($\theta = 0°$).

The primary purpose of using the GCPW-to-slotline transition instead of the traditional microstrip-to-slotline is to reduce the cross-polarization level. Fig. 2 shows the simulated E-field distribution at 18 GHz for different feeding structures. Compared with the microstrip line, the GCPW has a balanced E-field distribution, which can reduce the cross-polarization stemming from the asymmetric field distribution of the feeding line. The metallized vias of GCPW can reduce the radiation of the

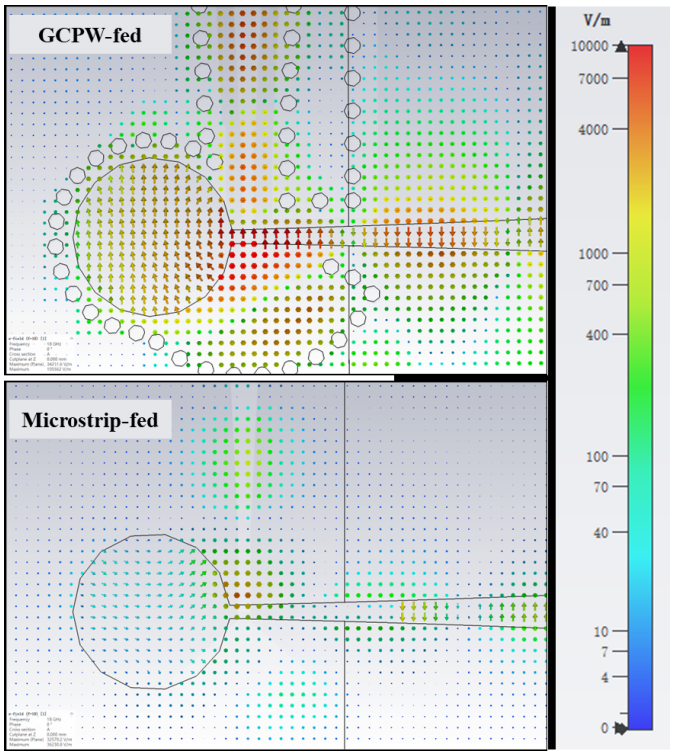

FIGURE 2. Simulated E-field distribution at 18 GHz.

GCPW-to-slotline transition structure, which also contributes to low cross-polarization.

The effects of different exponential curve coefficients and chamfer bending widths are investigated, as shown in Fig. 3. When the exponential curve coefficient increases from 0.036 to 0.056, the impedance matching gradually degrades in the low-frequency band below 6 GHz, while it gradually improves in the high-frequency band above 6 GHz. As can be observed from Fig. 3(b), with the increase of the chamfer bending width W_c, the $|S_{11}|$ in the low-frequency band below 4 GHz improves slightly, while the $|S_{11}|$ in the high-frequency band above 4 GHz degrades, which is exactly opposite to the trend of the exponential curve coefficient R.

In Fig. 4, the effects of the radial stub dimensions on $|S_{11}|$ are sketched. When R_1 is increased, the impedance matching improves within the 6–12 GHz range, but deteriorates in other frequencies. As the aperture angle (α) of the radial stub increases, the $|S_{11}|$ improves in the low-frequency band but degrades in the high-frequency band.

Figure 5 illustrates the CPRs of the different feeding structures at boresight ($\theta = 0°$) simulated using Computer Simulation Technology (CST) Microwave Studio. Compared with the traditional microstrip line feed structure, the GCPW feed structure can improve the CPR by 4–6 dB.

The proposed antenna achieves concurrent wide impedance bandwidth and low cross-polarization through the synergistic operation of three key geometric features. The wideband performance is primarily rooted in two aspects: First, the exponential flare of the main radiators functions as a smooth, graded impedance transformer, gradually matching the high input impedance at the feed point to the free-space wave impedance over 2–18 GHz. Second, the GCPW-to-slotline transition feed is inherently a wideband structure. The linear taper in the GCPW section provides controlled impedance transformation, while the circular cavity and radial stub act as broadband matching elements that suppress reflections across the target band.

The mechanism for low cross-polarization is distinctly tied to the balanced field excitation. As visualized in the simulated E-field distribution (Fig. 2), the GCPW feed confines the primary electric field between its center conductor and coplanar ground planes, creating a symmetric, in-plane field pattern at the launch point into the slotline. This balanced launch ensures that the currents excited on the two symmetric exponential arms are equal in magnitude and opposite in phase, promoting a pure, linearly polarized radiating wavefront in the principal plane. Crucially, the ten edge-loaded slots are not merely low-frequency enhancers; they also function as distributed tuning elements that help maintain this current symmetry along the flare edges as frequency varies, preventing the build-up of asymmetric current modes that are the primary source of cross-polarized radiation. Thus, the geometry enforces field symmetry from the feed point to the radiating aperture, effectively suppressing cross-polarization generation at its source across the entire operating bandwidth.

3. RESULTS AND DISCUSSION

To verify the design, a prototype antenna was fabricated as shown in Fig. 6. Radiation patterns, antenna gain, and cross-polarization were measured in an anechoic chamber (SATIMO StarLab system). The antenna under test was mounted on a positioning mast as the device under test. Prior to measurement, a full 2-port calibration of the vector network analyzer (Keysight N5224B) was performed at the coaxial cable ends using a standard electronic calibration module. The radiation patterns were acquired via a spherical near-field scanning technique and subsequently transformed to the far field.

Figure 7 depicts a comparison between the simulated and measured $|S_{11}|$ results. The measured impedance bandwidth, defined by the $|S_{11}| < -10$ dB criterion, spans from 2.01 GHz to 17.86 GHz, with a fractional bandwidth of 159.54%. It is noted that the $|S_{11}|$ response remains predominantly below -10 dB across this entire range, with minimal, localized excursions near -10 dB attributable to measurement uncertainty and connector effects. Besides, the -10 dB reference level is a widely accepted and practical criterion for defining the operational bandwidth of antennas, particularly in wideband systems, as it corresponds to a return loss of 90.1% and ensures minimal power reflection at the input port.

Figure 8 shows the simulated and measured radiation patterns of the proposed antenna in the E-plane (x-z plane, $\varphi = 0°$) and H-plane (y-z plane, $\varphi = 90°$) at four representative frequencies spanning the operational band (2, 6, 12, and 18 GHz), demonstrating stable pattern characteristics over a wide frequency range. As shown in Fig. 6, the measured co-polarized fields in the broadside direction exceed the cross-polarized counterparts by 34.68 dB, 15.71 dB, 12.43 dB, and

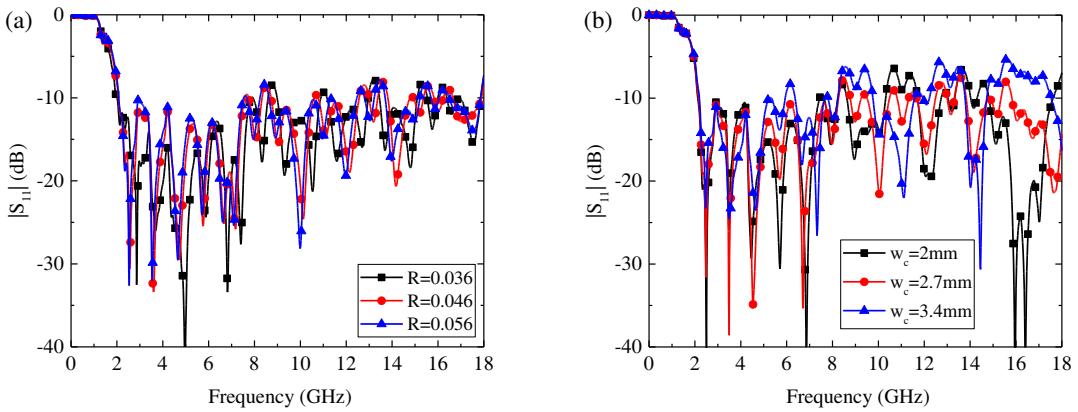

FIGURE 3. $|S_{11}|$ versus frequency for different coefficients of the exponential curve and chamfer bending width. (a) Different R, (b) different W_c.

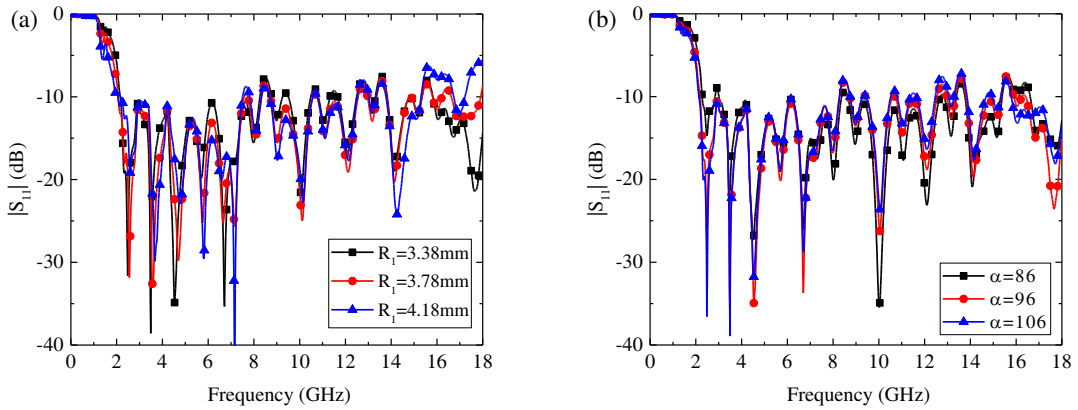

FIGURE 4. $|S_{11}|$ versus frequency for different radial stub dimensions. (a) Different out radius R_1, (b) different aperture angle α.

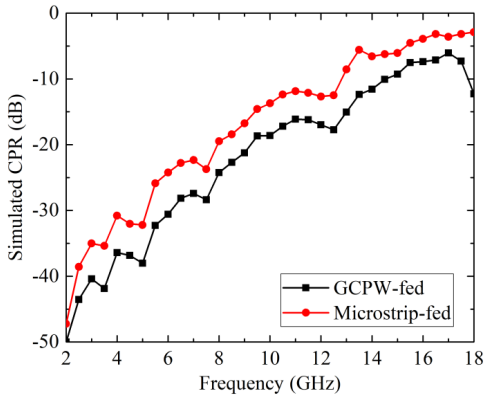

FIGURE 5. Simulated CPRs of different feeding structures.

13.18 dB at 2, 6, 12, and 18 GHz, respectively. The antenna has stable radiation patterns over a wide operating frequency band from 2 to 12 GHz. There is a deviation between the measured and simulated E-plane patterns above 12 GHz, which may result from the inaccurate line-widths of the GCPW and slotline limited by printed circuit board (PCB) machining accuracy. Another possible reason is that the length of the coaxial feed connector affected the high-frequency radiation pattern.

An observable trend in Fig. 8 is the gradual reduction in the separation between the co- and cross-polarized radiation patterns as the operating frequency increases. This frequency-dependent polarization characteristic can be attributed to two primary factors inherent to the traveling-wave nature of the Vivaldi antenna. First, at higher frequencies, the electrical size of the antenna aperture and its tapered slot increases. This leads to a more complex current distribution and the excitation of higher-order modes along the flare, which in turn generates more pronounced sidelobes and pattern distortion. These asymmetrical sidelobes contribute significantly to the cross-polarized field component in the far field. Second, the sensitivity to any residual structural asymmetry (e.g., from the feed transition or fabrication tolerances) is magnified at shorter wavelengths. Even minor imperfections that are electrically small at lower frequencies can become non-negligible sources of cross-polarized radiation at the upper end of the band. Consequently, while the fundamental radiation mechanism remains stable, the relative contribution of the cross-polarized component increases with frequency, leading to the observed decrease in polarization purity at higher GHz ranges.

The simulated and measured realized gains of the proposed Vivaldi antenna are shown in Fig. 9(a). The measured gain generally agreed with the simulation results. The measured gain was greater than 8 dBi from 3 to 8 GHz. However, as the frequency continued to increase, multiple sidelobes with higher gain appeared in the radiation pattern, resulting in a decrease

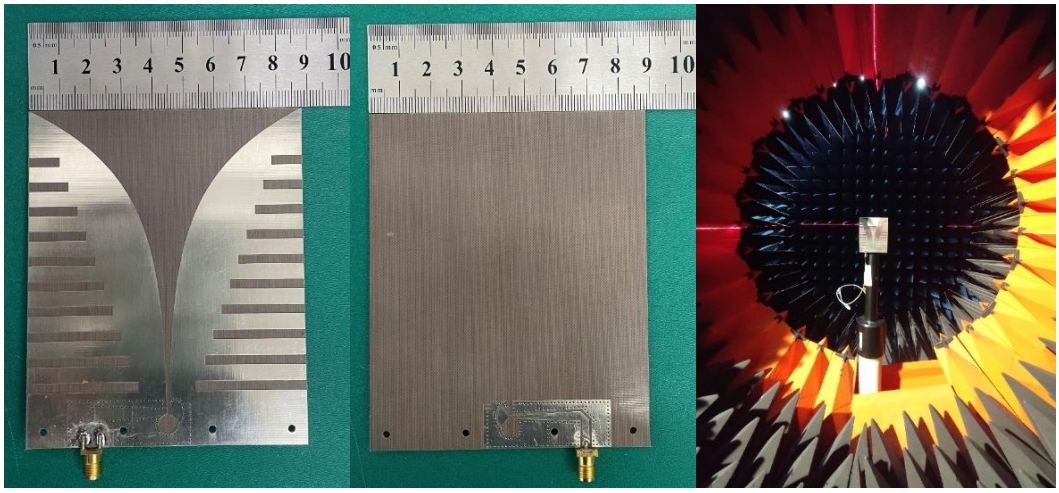

FIGURE 6. Photograph of the proposed GCPW-fed antenna and measurement setup.

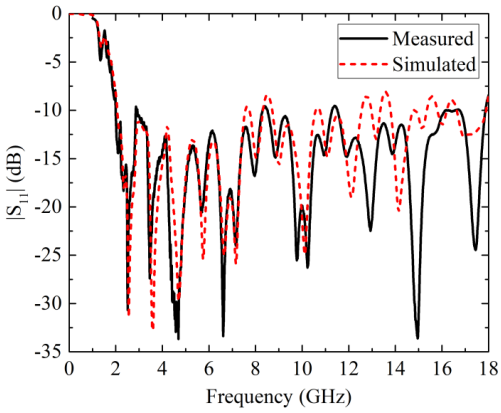

FIGURE 7. Simulated and measured reflection coefficient magnitudes of the proposed antenna.

in gain. Fig. 9(b) presents the antenna radiation efficiency; the measured radiation efficiency across the entire operating frequency band ranged from 74% to 94%. The discrepancy between the simulation and measurement may be attributed to additional losses introduced by the manual soldering of the SMA connectors.

Figure 10 shows the simulated and measured CPRs at boresight ($\theta = 0°$) across the operating band. The measured CPR remains below -20 dB from 2 to 12 GHz, with a maximum (worst-case) level of approximately -12.5 dB occurring around 17 GHz. The general trend of the measured CPR agrees with the simulation, though a consistent 5–10 dB degradation is observed. This degradation in measured cross-polarization performance is primarily attributed to practical imperfections introduced during fabrication and measurement, which are challenging to fully model in simulation. First, PCB fabrication tolerances (typically ± 0.1 mm for the used process) can lead to slight deviations in the critical dimensions of the GCPW gap and edge-loaded slots. These geometric variations subtly disturb the balanced E-field distribution maintained by the ideal GCPW structure, thereby elevating the cross-polarized component.

Second, the manual soldering of the SMA connector to the GCPW feed line can introduce minor asymmetry in the feed transition region. This asymmetry unbalances the otherwise symmetric current distribution, generating an unintended cross-polarized radiation. Finally, alignment uncertainties in the anechoic chamber measurement setup, despite careful calibration, can result in a small misalignment between the antenna's principal polarization plane and the reference axis of the receiving probe. This misalignment causes a portion of the strong co-polarized signal to be projected into the measured cross-polarized component, leading to an overestimation of CPR. It is noted that these practical factors collectively contribute to the observed discrepancy, while the overall trend and the significant improvement over the traditional microstrip-fed counterpart remain clearly validated.

Table 1 compares the performance of the proposed antenna with that of previously published research. Microstrip-line feed is a simple and common single-ended feed. However, its inherent asymmetric field distribution often leads to higher cross-polarization levels, as seen in [3] (-20 dB CPR). Differential feed inherently suppresses common-mode currents and can achieve good cross-polarization performance (e.g., -30 dB in [19]), but differential feed network adds complexity, potential loss, and can limit the achievable impedance bandwidth due to its symmetric excitation. Ref. [12] achieves outstanding simulated cross-polarization suppression (e.g., -40 dB) by enforcing field symmetry through a three-dimensional layout. This comes at the cost of significantly increased fabrication complexity, layer alignment requirements, and potentially higher weight and cost. Therefore, compared to the differential-fed antenna in [19], this work offers a much wider bandwidth (159.54% vs. 111%) using a single-ended feed. Furthermore, while matching the low cross-polarization levels approaching three-layer BAVA designs [11, 12], the proposed antenna maintains the cost and assembly advantages of a single-layer structure.

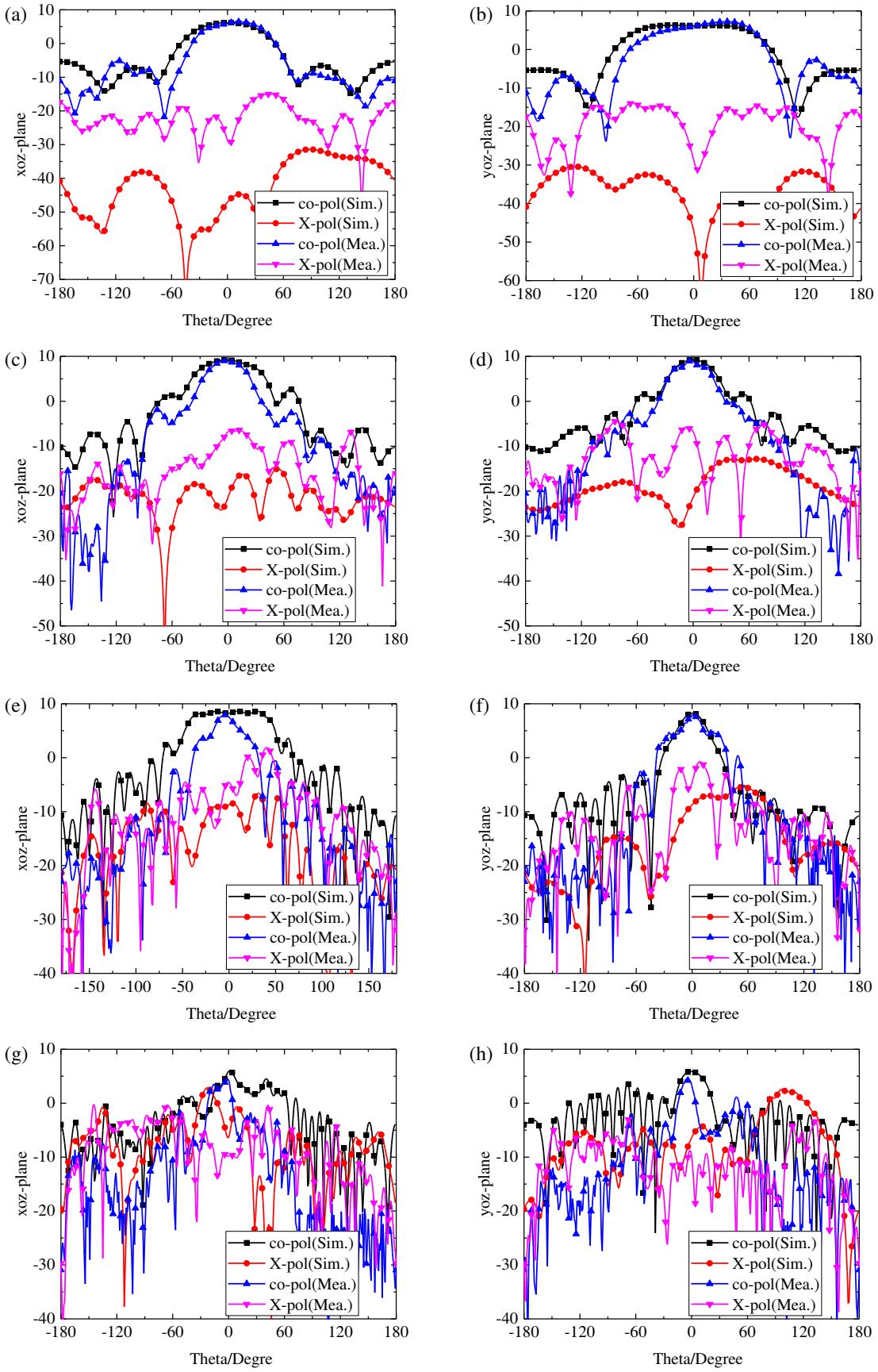

FIGURE 8. Simulated and measured radiation patterns. (a) (b) 2 GHz; (c) (d) 6 GHz; (e) (f) 12 GHz; (g) (h) 18 GHz.

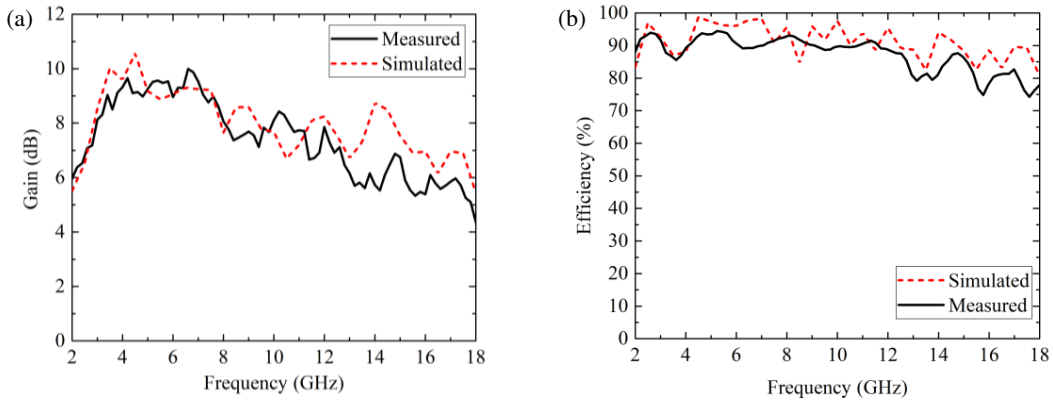

FIGURE 9. Simulated and measured realized gains and radiation efficiencies.

TABLE 1. Comparison between the proposed antenna and some references.

Ref.	Operating Frequency	Rrelative Bandwidth	Peak Gain	CPR	Radiation Efficiency	Normalized Electrical size	Number of dielectric layers	Feed type
[1]	55–84 GHz	41.70%	7 dB	—	80%	$0.42\lambda_L \times 0.55\lambda_L$	single-layer	Microstrip-line
[2]	2.5–8.5 GHz	109%	9.9 dB	—	—	$0.46\lambda_L \times 0.68\lambda_L$	single-layer	Microstrip-line
[3]	1.8–6 GHz	106%	>4 dB	-20 dB	—	$0.5\lambda_L \times 0.58\lambda_L$	single-layer	Microstrip-line
[11]	7–14.5 GHz	69%	3.75 dB	-20 dB	—	$0.28\lambda_L \times 0.6\lambda_L$	three-layers	FSIW
[12]	0.9–6 GHz	148%	9.53 dB	-40 dB (Simulated)	—	$0.21\lambda_L \times 0.6\lambda_L$	three-layers	Microstrip-line/ strip-line
[19]	2.0–7.0 GHz	111%	8.5 dB	-30 dB	—	$0.14\lambda_L \times 0.54\lambda_L$	single-layer	Differential
This work	**2.01–17.86 GHz**	**159%**	**9.9 dB**	**-35.3 dB**	**89%**	$\mathbf{0.59\lambda_L \times 0.72\lambda_L}$	**single-layer**	**GCPW**

(λ_L is the wavelength corresponding to the lowest frequency)

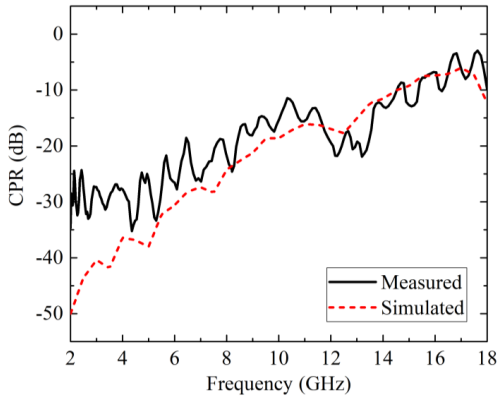

FIGURE 10. Simulated and measured CPRs.

4. CONCLUSION

A GCPW-fed Vivaldi antenna with low cross polarization is presented in this study. Benefiting from the balanced E-field distribution of the GCPW, the cross-polarization is 4–6 dB better than that of the traditional microstrip-fed Vivaldi antenna. Experimental and simulated results demonstrate that the proposed antenna can achieve a -10 dB impedance bandwidth of 15.85 GHz with stable radiation patterns. The proposed antenna has the advantages of ultra-wideband, low CPR, and high gain, and can be used in various broadband wireless information systems, such as UWB communication and multifunctional integrated RF systems.

ACKNOWLEDGEMENT

The study was supported by the Sichuan Science and Technology Program under Grant No. 2026NSFSC1417.

REFERENCES

[1] Ghaffar, F. A., N. K. Roy, and A. Shamim, "A single layer wideband Vivaldi antenna with a novel feed structure," *IET Microwaves, Antennas & Propagation*, Vol. 17, No. 7, 558–564, 2023.

[2] Ren, J., H. Fan, Q. Tang, Z. Yu, Y. Xiao, and X. Zhou, "An ultra-wideband Vivaldi antenna system for long-distance electromagnetic detection," *Applied Sciences*, Vol. 12, No. 1, 528, 2022.

[3] Zhang, K., R. Tan, Z. H. Jiang, Y. Huang, L. Tang, and W. Hong, "A compact, ultrawideband dual-polarized Vivaldi antenna with radar cross section reduction," *IEEE Antennas and Wireless Propagation Letters*, Vol. 21, No. 7, 1323–1327, 2022.

[4] Hossain, A. and A.-V. Pham, "A novel gain-enhanced miniaturized and lightweight Vivaldi antenna," *IEEE Transactions on Antennas and Propagation*, Vol. 71, No. 12, 9431–9439, 2023.

[5] Rodriguez-Garcia, P., J. Pierpont, J. Martin, E. Tobar, C. Weatherly, and R. George, "A lightweight, low-cost, S-ku band dual-

polarized antipodal Vivaldi antenna array for next-generation airborne systems," in *2023 IEEE Texas Symposium on Wireless and Microwave Circuits and Systems (WMCS)*, 1–5, Waco, TX, USA, 2023.

[6] Schaubert, D., E. Kollberg, T. Korzeniowski, T. Thungren, J. Johansson, and K. Yngvesson, "Endfire tapered slot antennas on dielectric substrates," *IEEE Transactions on Antennas and Propagation*, Vol. 33, No. 12, 1392–1400, 1985.

[7] Gibson, P. J., "The Vivaldi aerial," in *1979 9th European Microwave Conference*, 101–105, Brighton, UK, 1979.

[8] Gazit, E., "Improved design of the Vivaldi antenna," in *IEE Proceedings H (Microwaves, Antennas and Propagation)*, Vol. 135, No. 2, 89–92, 1988.

[9] Langley, J. D. S., P. S. Hall, and P. Newham, "Novel ultrawideband Vivaldi antenna with low crosspolarisation," *Electronics Letters*, Vol. 29, No. 23, 2004–2005, 1993.

[10] Zhang, W. T. and X. H. Zhang, "Design of a phased array element with low cross polarization," *Shipboard Electronic Countermeasure*, Vol. 43, No. 6, 101–104, 2020.

[11] Tang, Y.-C. and Z.-G. Wang, "Ultra-wide band balanced Vivaldi antenna using FSIW feeding structure," *Journal of Microwaves*, Vol. 30, 291–293, 2014.

[12] Wei, J., D. Meng, and X. Song, "Design of a miniature ultra-wideband antenna with low cross polarization," *Metrology Science and Technology*, Vol. 67, No. 2, 36–41, 2023.

[13] Natarajan, R., J. V. George, M. Kanagasabai, L. Lawrance, B. Moorthy, D. B. Rajendran, and M. G. N. Alsath, "Modified antipodal Vivaldi antenna for ultra-wideband communications," *IET Microwaves, Antennas & Propagation*, Vol. 10, No. 4, 401–405, 2016.

[14] Wang, Z., Y. Yin, J. Wu, and R. Lian, "A miniaturized CPW-fed antipodal Vivaldi antenna with enhanced radiation performance for wideband applications," *IEEE Antennas and Wireless Propagation Letters*, Vol. 15, 16–19, 2016.

[15] Lee, J. J., S. Livingston, and R. Koenig, "A low-profile wideband (5:1) dual-pol array," *IEEE Antennas and Wireless Propagation Letters*, Vol. 2, 46–49, 2003.

[16] Logan, J. T., R. W. Kindt, and M. N. Vouvakis, "A 1.2-12 GHz sliced notch antenna array," *IEEE Transactions on Antennas and Propagation*, Vol. 66, No. 4, 1818–1826, 2018.

[17] Kindt, R. W. and J. T. Logan, "Dual-polarized metal-flare sliced notch antenna array," *IEEE Transactions on Antennas and Propagation*, Vol. 68, No. 4, 2666–2674, 2020.

[18] Logan, J. T., R. W. Kindt, and M. N. Vouvakis, "Low cross-polarization Vivaldi arrays," *IEEE Transactions on Antennas and Propagation*, Vol. 66, No. 4, 1827–1837, 2018.

[19] Qi, H. and H. Liu, "Single-ended band-notched Vivaldi antenna with common mode suppression and low cross polarization," *IEEE Antennas and Wireless Propagation Letters*, Vol. 20, No. 10, 1983–1987, 2021.

[20] Stutzman, W. L., *Polarization in Electromagnetic Systems*, Artech House, 1992.